Received: 10 December 2020 | Accepted: 30 March 2021

DOI: 10.1002/vzj2.20130

Vadose Zone Journal

ORIGINAL RESEARCH ARTICLE

A black-box automated approach to calibrate numerical simulations and optimize cover design: Application to a flow control layer constructed on an experimental waste rock pile

Tom Crouzal[1,2] | **Thomas Pabst**[1,2]

[1] Dep. of Civil, Geological and Mining Engineering, Polytechnique Montreal, Montreal, QC H3T 1J4, Canada

[2] Research Institute of Mines and Environment (RIME), Montreal, QC H3T 1J4, Canada

Correspondence
Thomas Pabst, Dep. of Civil, Geological and Mining Engineering, Polytechnique Montreal, Montreal, QC H3T 1J, Canada.
Email: t.pabst@polymtl.ca

Assigned to Associate Editor Yonggen Zhang.

Abstract

Mining operations often produce large volumes of waste rock to access economically valuable mineralized zones. Waste rock is usually stored in surface piles, the construction and reclamation of which represent a challenge for the industry. A flow control layer (FCL) made of crushed waste rock or sand and constructed on top of each waste rock bench could contribute to control water infiltration, thus improving waste rock pile stability and limiting contamination. An experimental waste rock pile was built and instrumented at the Tio mine (Rio Tinto Fer et Titane, Canada) to evaluate the performance of an FCL in field conditions. Large infiltration tests and rainfall monitoring were carried out, and measured outflow and water contents were used to calibrate numerical simulations. However, data were noisy and sometimes incomplete, and the models were difficult to calibrate. A new automated calibration approach was therefore proposed. An algorithm was developed to automate the numerical simulation calibration, using a black-box method that involves solving an optimization problem on a function without an analytic form. The approach was applied on measurements obtained from large-scale infiltration tests and validated using 2 yr of field monitoring data. Finally, the automated approach was adapted to optimize the design of the FCL, and an optimal design (material properties and layer thickness) was recommended based on local climate conditions. The proposed automated method could contribute to reduce the bias induced by manual calibration and allows for rapid multivariable calibration and optimization for a broad spectrum of mine waste cover system applications.

1 | INTRODUCTION

Mining operations produce large volumes of waste rock to access economically valuable mineralized zones. Waste rock is characterized by a wide range of particle sizes, from metric blocs to clay size particles (Aubertin, Bussière, & Bernier, 2002; Trudinger & Spitz, 2008), and is usually stored in surface piles, whose height can exceed hundreds of meters and whose surface can cover dozens of hectares (Hawley & Cunning, 2017; McCarter, 1990). Waste rock piles are usually built on the surface and therefore exposed to atmospheric

Abbreviations: AMD, acid mine drainage; CND, contaminated neutral drainage; FCL, flow control layer; HGS, HydroGeoSphere; MADS, mesh adaptative direct search.

This is an open access article under the terms of the Creative Commons Attribution-NonCommercial-NoDerivs License, which permits use and distribution in any medium, provided the original work is properly cited, the use is non-commercial and no modifications or adaptations are made.
© 2021 The Authors. *Vadose Zone Journal* published by Wiley Periodicals LLC on behalf of Soil Science Society of America

conditions. The exposition of sulfide minerals (often contained in waste rock) to water and oxygen can result in acid mine drainage (AMD, characterized by low pH and high concentrations of sulfates and dissolved metals; Akcil & Koldas, 2006; Molson et al., 2005). Some sulfide minerals may also oxidize without producing acid, or acidity may be neutralized by carbonate minerals. In this case, the release of metals and metalloids such as As, Co, Ni, and Zn could contribute to generate contaminated neutral drainage or CND (Benzaazoua et al., 2013; Plante et al., 2010). Reclamation approaches to prevent AMD or CND generation usually involve cover systems that aim to control oxygen and/or water flux (Aubertin et al., 2016). Such techniques, including covers with capillary barrier effects (Aubertin et al., 2009) and elevated water table combined with monolayer covers (Aubertin et al., 2016; Pabst et al., 2017), were proven efficient to reclaim tailings storage facilities. However, reclamation of waste rock piles remains challenging, because of the size of the structures, the steep slopes (close to waste rock repose angle), and the deep water table (Aubertin et al., 2013).

A new method was, therefore, recently proposed to improve geochemical and geotechnical stability of waste rock piles during construction (progressive reclamation) and after closure (Aubertin, Bussière, Bernier, Chapuis, et al., 2002; Aubertin et al., 2013; Fala et al., 2005). This approach consists of building a flow control layer (FCL) on top of each bench of the pile. This FCL is made of compacted fine-grained materials, such as sand or crushed waste rock, and is inclined by around 5% towards the exterior of the waste rock pile. Fine-grained materials create a capillary barrier effect with the underlying coarse waste rock, therefore preventing downwards infiltration. The FCL slope enhances lateral diversion of water, thus preventing contacts with potential AMD/CND generating waste rock. More details about the FCL concept can be found in Aubertin, Bussière, Bernier, Chapuis, et al. (2002) and Broda et al. (2014). The method was validated at a large scale using an experimental waste rock pile built at the Tio mine (Rio Tinto Fer et Titane, QC, Canada). More details about the construction, properties, and monitoring of the experimental pile are given below.

Field data recorded in situ during a 2-yr monitoring period were then used to calibrate hydrogeological numerical simulations. The objective of numerical simulations was to extrapolate field results and optimize the FCL design, for this site and other mine sites with different climatic conditions.

Core Ideas

- Hydrogeological field measurement treatment was automatized before calibration.
- Numerical simulations of a flow control layer were conducted to optimize waste rock pile reclamation design.
- Calibration was automatized using a software based on MADS algorithm.

2 | CALIBRATION APPROACHES

Calibration, sometimes also referred to as inverse problem (He et al., 2013; Zhou et al., 2014), aims to determine unknown or uncertain model parameters (e.g., material hydrogeological properties such as porosity, hydraulic conductivity, or air entry value) based on experimental measurements (typically water contents, suctions, or water flow) to simulate as accurately as possible observed behavior (here hydrogeological flow). A trial and error approach is often used, where model parameters are manually changed after each simulation run until the results of the numerical simulation correspond well to the data measured in the field (Neuman, 1973). However, this approach often requires testing numerous combinations of parameters and can be time consuming (Carrera et al., 2005) and is sensitive to nonunique solutions and local optimums. Also, calibration can be contradictory, whereas some parameter modifications may improve some results but alter the quality of others (Zhou et al., 2014). Several improvements have therefore been proposed since, following the development of calculation tools.

Inverse problems are nowadays often automatized using algorithms to solve various types of calibration problems (Carrera et al., 2005; He et al., 2013; Zhou et al., 2014). The quality of data used for calibration remains of uttermost importance (Carrera et al., 2005; He et al., 2013). However, these are often deteriorated by time (sensors tend to have a limited service life). Moreover, the scale effect can also affect the quality of the calibration. Data are often obtained from local and punctual measurements such as boreholes, small lysimeters, and probes but are used to describe large-scale hydrogeological behavior and resolve continuous models (Emsellem & De Marsily, 1971; He et al., 2013; Zhou et al., 2014). The impact of local variations on the whole numerical model can therefore sometimes be exaggerated. The numerical model discretization needs to be adapted to those constraints, which often results in a significant increase in the computational time. Parallelization (Tavakoli et al., 2013) and surrogate models (Awotunde & Horne, 2011) can reduce the calibration time and are included in many different hydrogeological calibration problems such as geostatistical inversion and geological inversion (Carrera et al., 2005; Zhou et al., 2014). Nowadays, the software PEST is often used for solving such groundwater flow inverse problems (Doherty, 2015, 2018).

Using inverse approaches and optimization methods in unsaturated hydrogeology remains, however, complex

because of the nonlinearity of the material hydrogeological properties (such as the water retention curve or the permeability function) required to solve Richards' equation (Hollenbeck & Jensen, 1998). Recent developments in similar domains have proposed several approaches to tackle these challenges (Carrera et al., 2005; He et al., 2013; Zhou et al., 2014). For example, the approaches commonly used in geophysics aim to resolve an inversion to obtain the repartition of the bulk electrical resistivity to deduce the water content dimensional repartition (Carrera et al., 2005; Dimech et al., 2019), and spectral analysis can be used to determine transfer functions between inflow and outflow to represent the hydrogeologic behavior of a waste rock pile (Trinchero et al., 2011). These methods work well to represent the heterogeneity of a hydrogeologic system, but they are dependent of an analytic form between those measurements and the properties of the materials (Turunen et al., 2020). Various studies also proposed to use metaheuristics optimization methods to resolve inverse problems without a direct analytic objective function (Abbaspour et al., 2001). Metaheuristic algorithms are mathematical functions that search for the best neighborhood solution. Monte Carlo and ant-colony algorithms are among the most common metaheuristics approaches (Abbaspour et al., 2001; Zhou et al., 2014). An ant-colony algorithm was, for example, used to calibrate the water retention curve in an experimental soil cover based on field measurements of the pressure head (Abbaspour et al., 2001). The convergence of metaheuristics methods is not mathematically proven and requires a large number of iterations to obtain an optimal solution. Such an approach may therefore not be adapted when the objective function is based on time-consuming numerical simulations. To solve this issue, nonheuristic and derivative-free optimization methods were proposed. These methods, also referred to as black-box approaches, are particularly interesting for time-consuming groundwater models or nonlinear problems (Mugunthan et al., 2005). Nomad software, a derivative-free algorithm developed by Gerad (*Groupe d'Études et de Recherche en Analyse des Décisions*, Polytechnique Montreal) to resolve black-box optimization and shorten the number of iterations (Audet & Hare, 2017) was used in this study.

Black-box optimization aims to resolve a nonderivative and noncontinuous function with no analytical equation (Audet & Kokkolaras, 2016). The solver is based on derivative free mathematics and mesh algorithm (Audet & Hare, 2017; Audet & Kokkolaras, 2016). The mesh adaptative direct search (MADS) algorithm used in the black-box optimization is an iterative algorithm generating trial points on a mesh. The mesh represents the entry variable discretization space to resolve the black-box functions. The step size between each iteration in the MADS algorithm is defined by two parameters: the mesh size parameter Δ_k^m and the poll size parameter Δ_k^p (Audet, 2014). The mesh size parameter defines the coarseness or fineness of the mesh M^k as

$$M_k = \left\{ x + \Delta_k^m D_z \; x \in V_k, z \in \mathrm{N}^{n_D} \right\} \subset \mathrm{R}^n \tag{1}$$

where V_k is the current iteration, $\Delta_k^m \in \mathrm{R}^+$ is the mesh size, n is the number of directions, and D_z is a fixed set of n_D directions in N.

The poll set P_k defines the trial points inside the mesh M_k corresponding to mesh points distant from x_k using a bound set by a constant $c > 0$ applied on the poll size parameter Δ_k^p (Audet, 2014):

$$P_k \subseteq x \in M_k \; x - x_k \leq c\Delta_k^p \tag{2}$$

The iterations process starts with a user-defined starting point $x_0 \in \mathrm{R}^n$ with $f(x_0) < \infty$, and initial mesh and poll size parameters (typically $\Delta_0^m = \Delta_0^p = 1$) (Audet, 2014). The algorithm iterates the functions SEARCH and POLL to evaluate trial points and determine the most feasible one. The algorithm updates a new starting point V_{k+1} and the mesh and poll size parameters Δ_{k+1}^m and Δ_{k+1}^P until the stopping criteria are met.

The black-box optimization approach was successfully used in several projects in civil engineering, for example, to optimize seismic dumper (Bigdeli et al., 2012), to calibrate a source and sinks numerical model (Guay et al., 2015), and to optimize well design (Isebor et al., 2014). The Nomad software was also used to calibrate regional hydrological models (Arsenault & Brissette, 2016; Minville et al., 2014) and was proven more efficient than other optimization methods in some cases (Fowler et al., 2008). The main advantages of Nomad are (a) the MADS algorithm that can reduce the kriging interpolation error (Alarie et al., 2013), and (b) the metaheuristic resolutions that can resolve optimization problem without the computation of the gradient and/or the Laplacian, thus shortening calculation time by limiting the number of iterations (Minville et al., 2014; Muguntham et al., 2005).

In this study, the black-box optimization approach was used to calibrate the numerical simulations of the experimental waste rock pile at Lac Tio mine. Waste rock and cover materials hydrogeological properties (i.e., water retention curve and saturated hydraulic conductivity) were calibrated to simulate the volumetric water content variations measured in the waste rock pile. Calibration was carried out on data collected during large-scale infiltration tests (see below) and validated using 17 mo of field monitoring. The same black-box approach was then adapted to optimize the cover design and improve its performance.

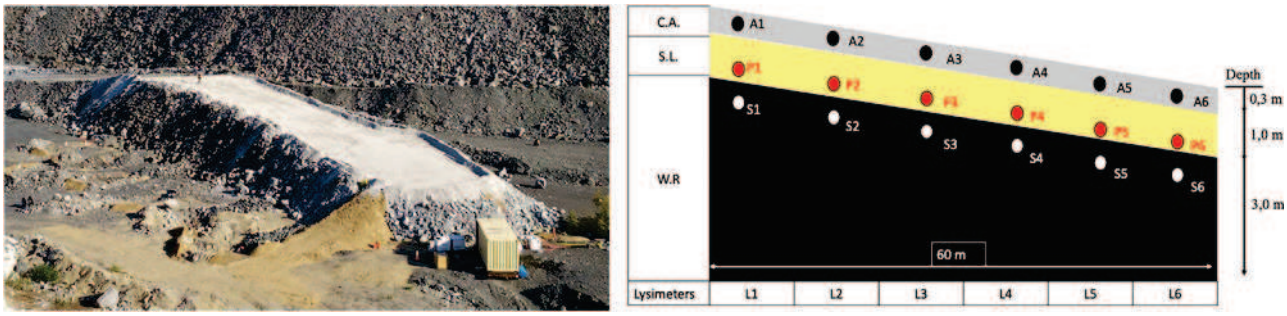

FIGURE 1 (a) Experimental waste rock pile at Lac Tio mine (credits: RIME) and (b) simplified cross section of the waste rock pile with instrumentation. The experimental pile was 70 m long and 10 m wide, with a maximal height of 7 m and a 5% slope (towards the bottom right of the picture). Waste rock (WR) was covered by a 0.7-m-thick sand layer (SL) and a 0.3-m-thick crushed anorthosite layer (CA). Locations of GS3 probes are shown with color points. A1–A6 sensors (black), P1–P6 sensors (red), and S1–S6 sensors (white) were placed 0.25, 0.80, and 1.30 m below the surface, respectively. Lysimeter positions (L1–L6; see text for details) are also shown

3 | METHODOLOGY

3.1 | Experimental waste rock pile and field monitoring data

An experimental pile was built and instrumented at the Tio mine (Rio Tinto Fer et Titane, Quebec, Canada) to evaluate the performance of a FCL at a large scale and in real field conditions (Figure 1) (Martin et al., 2017,2019).

The experimental waste rock pile was 70 m long and 10 m wide (Figure 1). The maximum height was 7 m and the surface of the pile was inclined with a 5% slope. The FCL was made of a 0.6-m compacted sand layer covered by a 0.3-m layer made of crushed anorthosite. The core of the experimental waste rock pile was made of CND-generating ilmenite waste rock. Nonreactive anorthosite (i.e., noncontaminating) waste rock was placed in the last ten meters (x = 60–70 m), where water was expected to infiltrate after deviation. Flow control layer and waste rock hydrogeological properties were evaluated in situ and in the laboratory. The FCL sand was characterized by a saturated hydraulic conductivity between 9×10^{-4} and 2×10^{-2} m s^{-1}, an air entry value of 2 kPa, and a water entry value of 11 kPa (Bréard Lanoix et al., 2020). The crushed anorthosite had a hydraulic conductivity around 5×10^{-4} m s^{-1}, with an air entry value of 1 kPa and a water entry value around 13 kPa (Dubuc et al., 2017). The saturated hydraulic conductivity of both ilmenite and anorthosite waste rock was approximately 1×10^{-3} m s^{-1} (Dubuc et al., 2017; Peregoedova et al., 2013), with an air entry value between 0.2 and 0.7 kPa, and a water entry value around 6 kPa (Dubuc et al., 2017; Peregoedova et al., 2014). These values are averages and, in practice, both ilmenite and anorthosite waste rock showed some heterogeneity in situ.

Hydrogeological response of the system to climatic conditions was monitored between April 2016 and September 2017. Six large scale infiltration tests (I-A to I-E) were also conducted to evaluate the pile hydrogeological response under controlled conditions (Dubuc et al., 2017). Tests I-C and I-D reproduced large precipitation events, with 28 m^3 (47 mm) and 16.8 m^3 (28 mm), respectively, sprayed at the surface of the experimental waste rock pile with a water truck over 10 h (Dubuc et al., 2017; Martin et al., 2019). Six lysimeters were built at the bottom of the pile (Figure 1b) to collect and measure water outflow and characterize water quality (not discussed here; see Poaty et al., 2018). Water content probes (GS3; Decagon Devices) were installed 0.80 m (sand) and 1.30 m (waste rock) below the surface every 10 m along the centerline of the waste rock pile (Figure 1b; Broda et al., 2017; Martin et al., 2017). Water contents were recorded every 15 min for all the monitoring period. Measures recorded at 0.80-m depth during tests I-C and I-D (from 7 to 20 June) are presented in Figure 2 and are typical of the hydrogeological response of the system to infiltration. Water contents were initially low around 0.10 and rapidly started to increase 4.5 h after test I-C started. Water content reached a peak (around 0.17) approximately 10.3 h after the beginning of the infiltration test, and then started to decrease again, but more slowly, towards its initial value. The hydrogeological response of the FCL was similar for test I-D (Figure 2) and other precipitation events, but the amplitude of the peak depended on the precipitation intensity.

3.2 | Data treatment

Volumetric water content data were noisy and difficult to integrate directly into a calibration process (Figure 2). Data were therefore treated to facilitate the automation of the calibration. First, the noise was filtered by applying a spectral low-pass filter on the water content time series (Figure 3). The objective was to damp small water content variations and to increase the precision of the computation of the wetting front arrival time. The spectral filter cut the frequencies higher than 2.3×10^{-5} Hz, which corresponded to a periodic variation

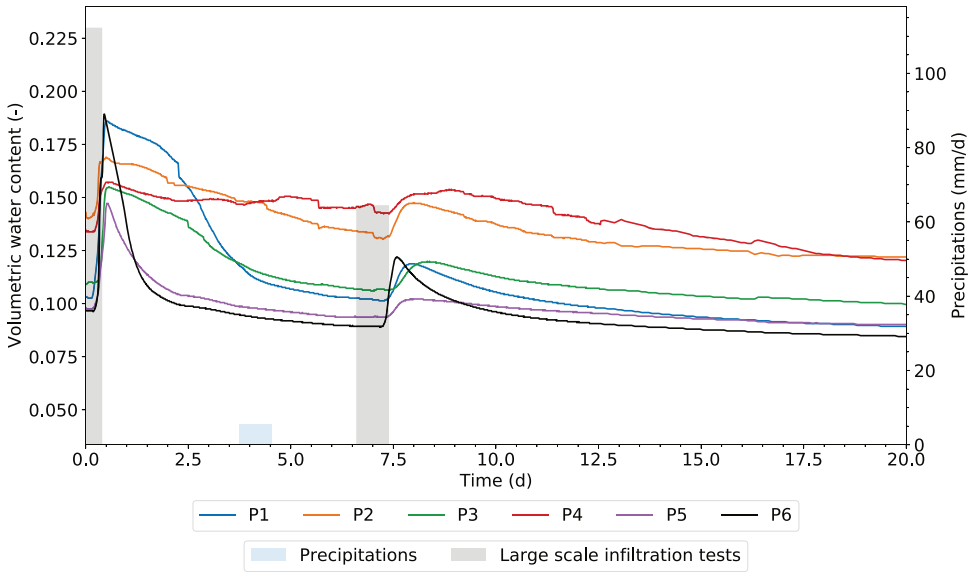

FIGURE 2 Measured volumetric water content 0.80 m below the surface and at different locations along the experimental pile (see Figure 1 for the position of probes P1 to P6). Precipitations are represented in blue and the large infiltration tests I-C and I-D in gray. Time $t = 0$ d corresponds to the start of test I-C (i.e., 7 June 2016). Test I-D started at Day 7 (i.e., 14 June 2016)

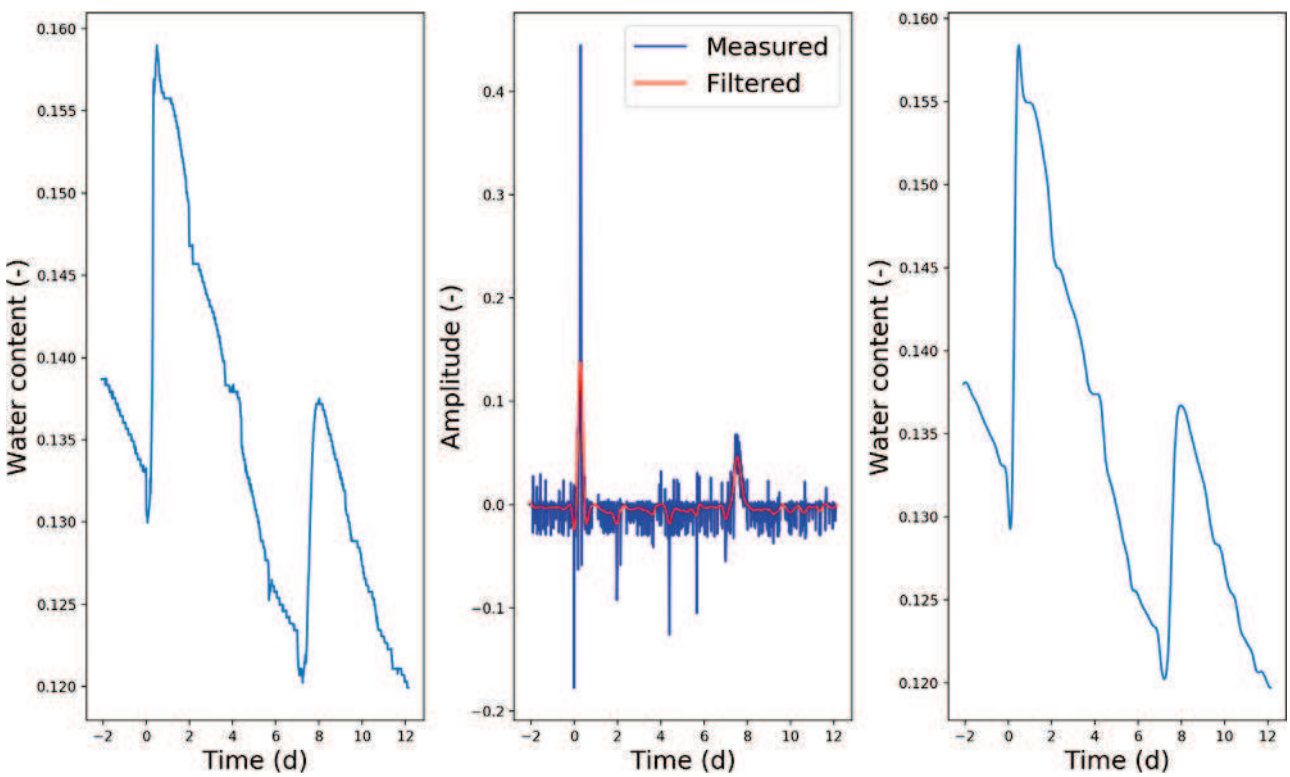

FIGURE 3 (a) Volumetric water content variations measured at P2 (0.80 m below the surface; see Figure 1b for sensor location) during tests I-C and I-D; (b) variation frequency with low pass spectral filtration to remove periodic variation below 0.5 d (see text for details); and (c) filtered water content variations used to determine the arrival time of the wetting front. The same filter was applied to the other measurements

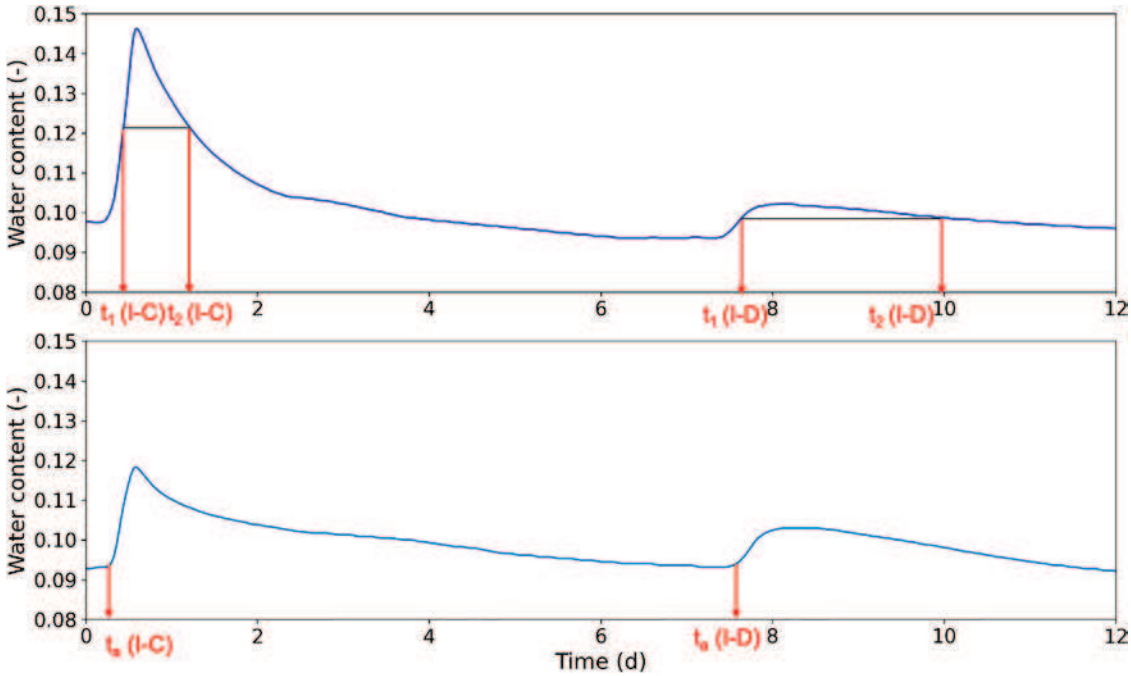

FIGURE 4 (a) Determination of parameters t_1, t_2 for sensor P5 (0.80 m below the surface, in the flow control layer [FCL]) during tests I-C and I-D; (b) determination of t_a (arrival time) for sensor S5 (1.30 m below the surface) during tests I-C and I-D

of 0.5 d (Figure 3b). Filtered water contents were very close to raw measurements, but some variations were exaggerated, which were beneficial to automatically determine arrival time (Figure 3c).

Three characteristic parameters were then chosen to represent the variations of the volumetric water content in the FCL and waste rock. Time t_1 corresponded to the time required to reach 50% of the maximum increase (peak) of the volumetric water content induced by the infiltration (Figure 4). Time t_2 corresponded to the time necessary to reach 50% of the difference between the maximum and minimum volumetric water content during drainage. Time t_a corresponded to the arrival time of the wetting front in the waste rock, 1.3 m below the surface. Parameters t_1, t_2, and t_a were determined for each probe and both tests I-C and I-D.

These parameters were chosen to limit the number of comparison points and accelerate the automated calibration process, and to normalize the comparison of less biased data to reproduce the water content variations. Times t_1 and t_2 were directly linked with the wetting front passage and the drainage velocity. Wetting front arrival time t_a in the waste rock was a useful indication of the water behavior at the interface between the FCL and the waste rock. The reduction of comparison parameters (instead of using the whole water content time series), also permitted to limit the risk for underfitting that may occur for high variance problems and which often results in a linear and nonrepresentative solution (Fienen et al., 2009; Poeter & Anderson, 2005). Finally, the chosen calibration parameters were not mathematically derived from Richards' equation, thus allowing for a more flexible optimization algorithm that could be more easily reused in the optimization objective function (see below).

3.3 | Numerical simulations

In this study, the equivalent porous media approach was used to simulate water flow in the experimental waste rock pile implicitly assuming that waste rock, sand, and crushed waste rock were homogeneous. The numerical simulations were carried out using the software HydroGeoSphere (HGS, Aquanty). The HGS resolves the three-dimensional Richards' equation for subsurface flow using the control volume finite element approach (Brunner & Simmons, 2012).

The geometry of the waste rock pile was simulated as a 60-m by 10-m trapezoid, with a maximal height of 7 m and a surface slope of 5%, mimicking the experimental waste rock pile in the field (see above). The mesh was formed of hexahedral structured blocks of 0.25 m × 0.25 m × 0.20 m. Mesh was refined to 0.25 m × 0.25 m × 0.06 m in the FCL. Mesh was optimized to ensure convergence and flow stability, while minimizing calculation time.

Material properties included the saturated hydraulic conductivity and van Genuchten (1980) parameters to describe the water retention curve. Initial properties were obtained based on laboratory and field measurements (see below). The saturated water contents of the FCL sand, the waste rock and the crushed anorthosite were respectively 0.33, 0.25, and

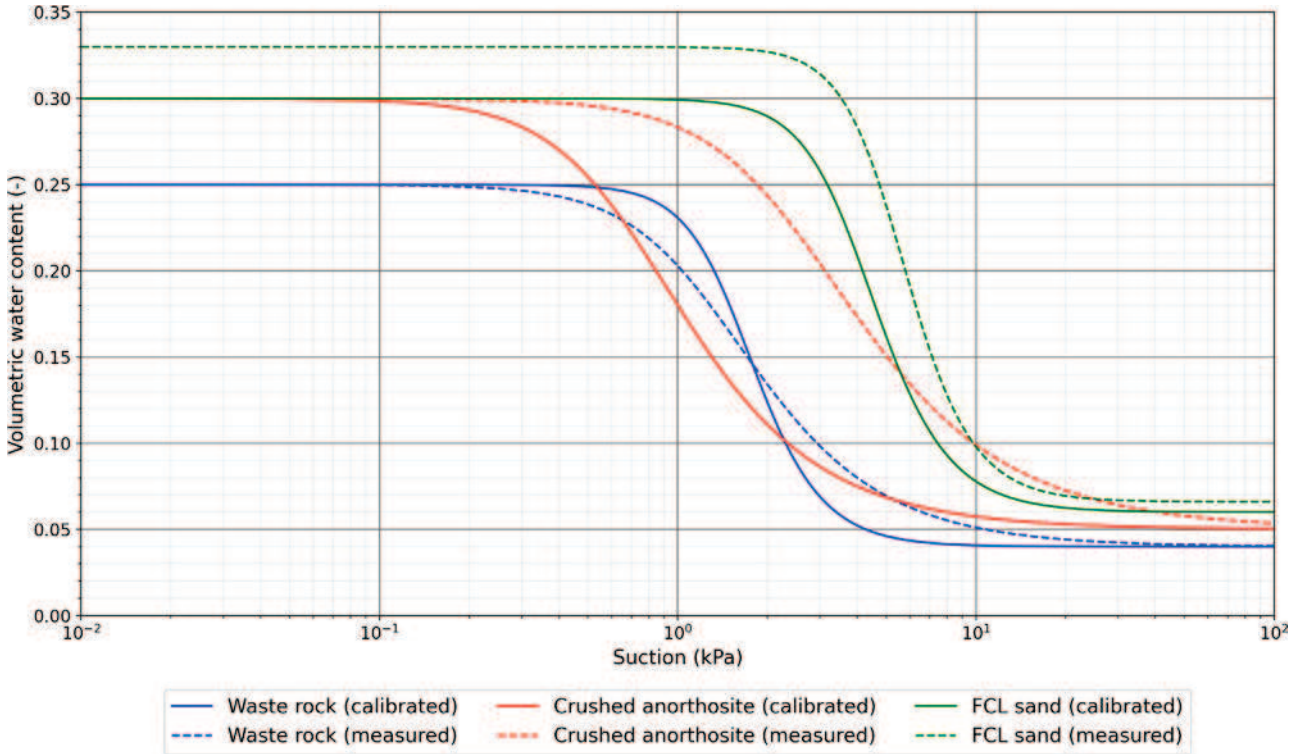

FIGURE 5 Measured (dashed lines) and calibrated (solid lines) water retention curves of the waste rock (blue), flow control layer (FCL) sand (green), and crushed anorthosite (red) in the experimental waste rock pile (Bréard Lanoix et al., 2020; Dubuc, 2018)

0.30 (0.04, 0.07, and 0.06 for the residual water contents; Figure 5). The residual and saturated water contents of the FCL sand were manually decreased to correspond to in situ measurements with a nuclear density gauge (Bréard Lanoix et al., 2020).

Initial conditions were defined as hydrostatic conditions. The simulations then computed the 38 d before the start of test I-C to simulate more realistic initial conditions before the large infiltration tests. The boundary condition at the bottom of the waste rock pile was a fixed pressure head of 0 m to simulate the position of the water table in the lysimeters. At $x = 60$ m, a vertical seepage face simulated a Neumann boundary to ensure the continuity of the water flow towards the exterior of the waste rock pile. At $x = 0$ m, an impermeable condition was fixed to represent the watershed. Infiltration tests and precipitations were simulated by applying a unit flux condition on the top boundary.

3.4 | Automated calibration approach

Numerical simulation results were extracted, and simulated and measured t_1, t_2, and t_a were compared by calculating the mean value of the quadratic error:

$$e_{\text{sum}} = \frac{\sum_{i=o}^{n} \left(p_i - p_i^*\right)^2}{n} \tag{3}$$

Where p_i is a measured parameter, p_i^* is a simulated parameter, and n is the number of parameters. Parameters p_i in Equation 3 corresponded to t_1 and t_2 at locations P1 to P6 and t_a at locations S1 to S6, during tests I-C and I-D. In total, 36 parameters were used for the comparison.

The objective of the optimization was to minimize the value of e_{sum} by varying the input properties (i.e., the hydraulic conductivity, α_{VG}, and n_{VG} for each of the three materials). The hydrogeological properties were calibrated individually and were bounded to correspond to a realistic range of properties for the different materials composing the waste rock pile (Table 1). For example, the minimum and maximum saturated hydraulic conductivity of the FCL was 5×10^{-6} m s^{-1} and 1×10^{-3} m s^{-1} respectively, typical values for a sand (Hillel, 1998). The porosity and the residual water content had been extensively measured in the field using various approaches (Dubuc, 2018; Bréard-Lanoix et al., 2020) and were therefore not calibrated here.

The software Nomad (Le Digabel, 2011) was used for the calibration. Nomad is a mesh adaptative detection search (MADS) software developed to resolve black-box optimization (Audet & Dennis, 2006). Nomad is a user-friendly software using a pseudo-code that can be embedded in a Python code.

A surrogate function (He et al., 2013; Le Digabel, 2011; Minville et al., 2014) was also developed, based on the same algorithm. The surrogate should meet two criteria: (a) be

TABLE 1 Lower and higher bound used during the calibration of the numerical simulation

Materials	Bound					
	k_{sat}		α_{vG}		n_{vG}	
	Low	High	Low	High	Low	High
	m s^{-1}		m^{-1}			
Crushed anorthosite	7×10^{-6}	1×10^{-4}	0.03	50	1	40
FCL sand	5×10^{-6}	1×10^{-3}	0.03	50	1	40
Waste rock	2×10^{-4}	5×10^{-2}	0.03	50	1	40

Note. k_{sat}, saturated hydraulic conductivity; α_{vG} and n_{vG}, van Genuchten (1980) fitting parameters. FCL, flow control layer.

TABLE 2 Initial and calibrated material properties in the numerical simulations of the experimental waste rock pile

Properties	Measured			Calibrated (e_{sum} = 0.019)		
	Crushed anorthosite[a]	FCL sand[b]	Waste rock[a]	Crushed anorthosite	FCL sand	Waste rock
k_{sat}, m s^{-1}	5×10^{-4}	9×10^{-5}	5×10^{-3}	9×10^{-6}	1×10^{-4}	2×10^{-2}
α_{vG}, m^{-1}	3.98	1.25	7.75	13.79	2.44	6.16
n_{vG}	2.16	6.00	2.34	2.34	3.89	4.13

Note. k_{sat}, saturated hydraulic conductivity; α_{vG} and n_{vG}, van Genuchten (1980) fitting parameters. FCL, flow control layer. e_{sum}, mean value of the quadratic error.
[a]Dubuc (2018).
[b]Bréard-Lanoix (2017).

similar to the principal objective function, and (b) possess a shorter calculation time (Audet & Hare, 2017). The surrogate permitted to shorten the optimization process and to find trial points quicker. In concrete terms, the numerical simulations running time was decreased in the surrogate function by applying a precipitation function of only 12 d instead of 60 d and by increasing the grid size (0.25 × 0.25 × 0.50 m inside the waste rock, 0.25 × 0.25 × 0.18 m and 0.25 × 0.25 × 0.08 m for the FCL sand layer and the crushed anorthosite layer). Also, the calculations were faster by using the parallelization option in HGS software (He et al., 2013; Le Digabel, 2011).

4 | RESULTS

4.1 | Material properties

The black-box algorithm iterated an important number of possible hydrogeologic properties until it converged (i.e., before the value of e_{sum} was minimum). The solution obtained had an error $e_{sum} = 0.019$. The calibrated saturated hydraulic conductivities for the sand of the FCL and the waste rock were somewhat greater than measured (Table 2), but differences were limited and smaller than one order of magnitude. The calibrated hydraulic conductivity of the crushed anorthosite was around one order of magnitude smaller than the measured value in the laboratory. This difference could be explained (in part) by the significantly higher density observed in situ (Dubuc, 2018).

The calibrated water retention curves for the sand and the waste rock were relatively similar to the curves estimated from previous studies (Figure 5). For example, the calibrated water retention curve for waste rock was slightly steeper than the initial curve (indicating a material with a somewhat smaller coefficient of uniformity), but the air entry value was similar and around 1 kPa. The difference between initial and calibrated curves for crushed anorthosite was more marked. The air entry value and the water entry value decreased to 0.5 and 4 kPa, which marked a smoother retention curve for the crushed anorthosite. The differences between measured and calibrated hydrogeological properties of the crushed anorthosite can mainly be explained by the limited number of characterization tests carried out in the field and in the laboratory (significantly less than for the sand and the waste rock), and the natural heterogeneity of the material.

4.2 | Arrival times and water content variations

In general, calibrated simulations were able to reproduce relatively well the measured variations of volumetric water content in the FCL: a quick and sharp increase of the water content a few hours after the beginning of the infiltration test (Table 3), followed by a slow decrease of the water content towards its initial value (Figure 6).

Simulated arrival times in the FCL (sensors P1 to P6) were generally slightly greater than the measured ones, with a mean

TABLE 3 Wetting front arrival times after the beginning of test I-C in the flow control layer (FCL, 0.8 m below the surface) and in the waste rock (1.3 m below the surface). The peak arrival time at 0.80-m depth is also compared

	Arrival time at 0.8-m depth		Time at maximal amplitude at 0.8-m depth		Arrival time at 1.3-m depth	
x	Measured	Calibrated	Measured	Calibrated	Measured	Calibrated
m	h					
5	3.58	6.67	11.75	13.31	N/A[a]	N/A
15	3.91	6.69	8.18	13.39	5.79	9.60
25	6.00	6.82	12.10	13.58	6.60	9.63
35	N/A	N/A	N/A	N/A	6.30	9.52
45	5.10	6.93	12.32	14.04	5.84	9.18
55	5.15	6.66	10.74	13.57	N/A	N/A
Mean delay	N/A	1.81	N/A	2.81	N/A	3.35

[a]NA, not applicable.

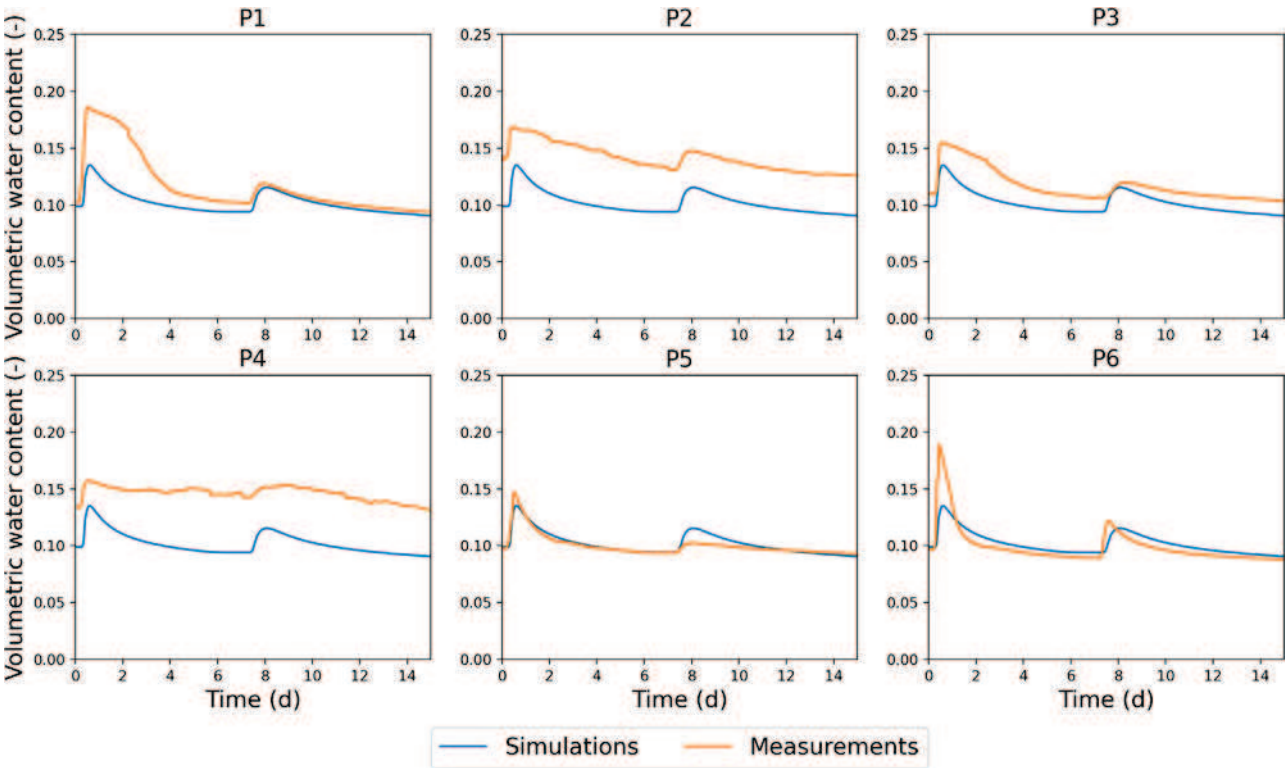

FIGURE 6 Measured (orange curve) and simulated (blue curve) volumetric water content 0.80 m below the surface after large scale infiltration tests I-C (day = 0) and I-D (day = 7)

delay of 1.8 h for test I-C (Table 3) and 2.1 h for test I-D. The simulated maximum (peak) water content was also reached later in the simulations than in the field, with a delay of 2.8 h for test I-C and 3.5 h for test I-D. The arrival time in the waste rock (sensors S1 to S6) was between 5.8 and 6.6 h after the beginning of test I-C corresponding to a mean delay of 3.4 h compared with measured arrival times (Table 3). The result for test I-D was similar with a mean delay for test I-D around 3.4 h. The delays observed with noncalibrated simulations were two to three times higher, showing the importance of calibration.

The simulated and measured initial water contents were slightly different depending on the position of the sensors in the experimental waste rock pile, and it was therefore deemed more representative to compare the relative increase of water content than the maximum (peak) values. For most of the sensors, measured trends and variation amplitudes of water contents were well simulated by the calibrated simulations

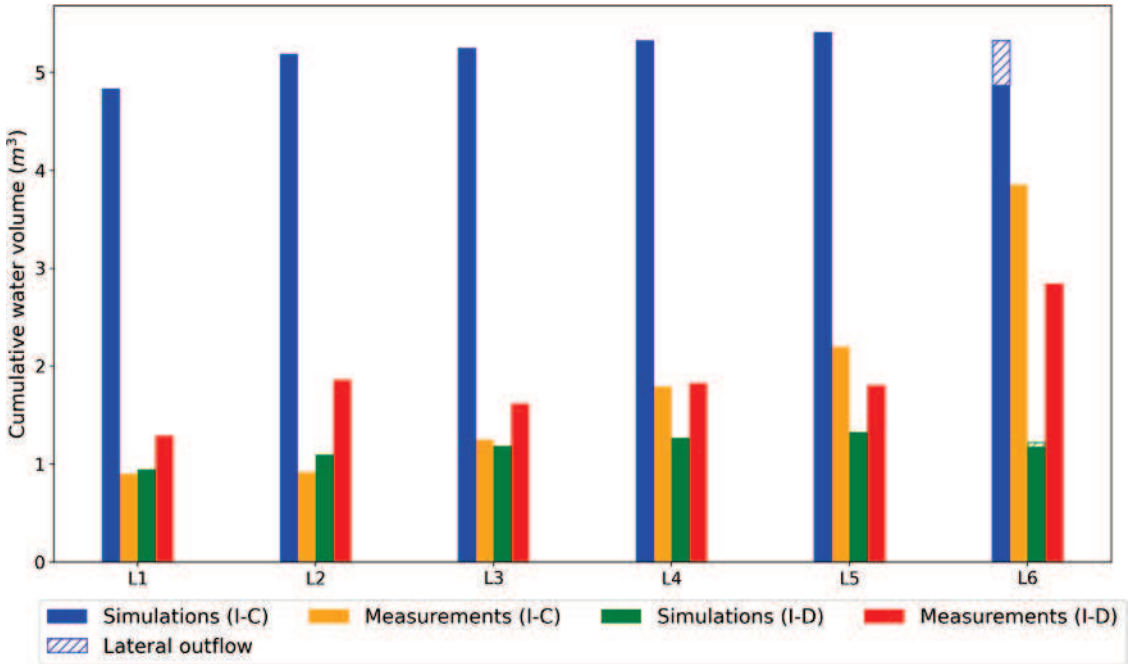

FIGURE 7 Simulated and measured cumulative water volumes leached at the bottom of the waste rock 7 d after test I-C. and 7 d after test I-D

(Figure 6). For example, simulated water content at P5 during tests I-C and I-D were very similar to measured data, with a maximum difference not exceeding 0.015 (sensor precision is 0.03). The difference between measured and calibrated water content for P2 and P3 corresponded to a constant offset of 0.04 and 0.015, respectively, but the variations were otherwise almost identical. Larger differences were observed for P1 and P6, but the measured increase of water content during infiltration test I-C was also significantly greater than that for the other sensors in the FCL. Simulated water contents for P1 and P6 during test I-D were very similar to measured results.

For P1, P2, and P3, the simulated volumetric water content decreased (after the peak) slightly faster than the measured curve, whereas for P6, the simulated decrease was slightly slower than the measured one. However, in all cases, the numerical simulations tended to an (almost constant) equilibrium water content of 0.09 at the end of the drainage phase for test I-C and test I-D, which was similar to the initial water content before the beginning of the infiltration tests. This trend was similar to measured water contents which also decreased towards their initial value (between 0.13 at P2 and 0.09 at P6), around 6.5 d after test I-C and 5.5 d after test I-D.

Measurements at P4 showed a slightly different behavior from the other sensors. Water content also increased a few hours after the beginning of both infiltration tests I-C and I-D but decreased significantly more slowly with a lot of small variations (which could not be completely removed by the low pass filter). Results seem therefore to indicate a greater water retention capacity in this zone of the FCL, which was not possible to reproduce with the model (materials were assumed homogeneous, see above).

Results for other locations in the experimental waste rock pile (i.e., crushed anorthosite and waste rock) were similar to the FCL.

Overall, and despite some limited discrepancies between simulated and measured water contents, calibrated models were able to simulate relatively well the hydrogeological behavior of the experimental waste rock pile after large infiltration tests. Numerical simulations matched the measured variations for some sensors and periods and represented an acceptable compromise for the others (especially considering the local heterogeneities and the precision of the sensors).

4.3 | Water fluxes in lysimeters

Simulated cumulative water fluxes in the lysimeters were compared to field measurements (Figure 7). For test I-C, both measured and simulated water fluxes increased progressively with the distance; for example, water fluxes in lysimeter L5 was greater than in L4, which was greater than in L1. However, simulated cumulative water volumes in lysimeters L1 to L5 were four to five times greater than measured ones, with a mean difference of 3.8 m^3. The difference between lysimeters was also more important in the field. For example, measured water flux was 0.9 m^3 in L1 and 2.2 m^3 in L5 (+1.3 m^3), but simulated water flux was 4.8 m^3 in L1 and 5.4 m^3 in L5 (+0.6 m^3). These trends were similar for test I-D. The recovery percentage (i.e., the ratio of water recovered in the lysimeters compared with the amount of water infiltrated at the surface) for test I-C was 110% for the calibrated simulations and only 39% for the measurements. On the contrary, the

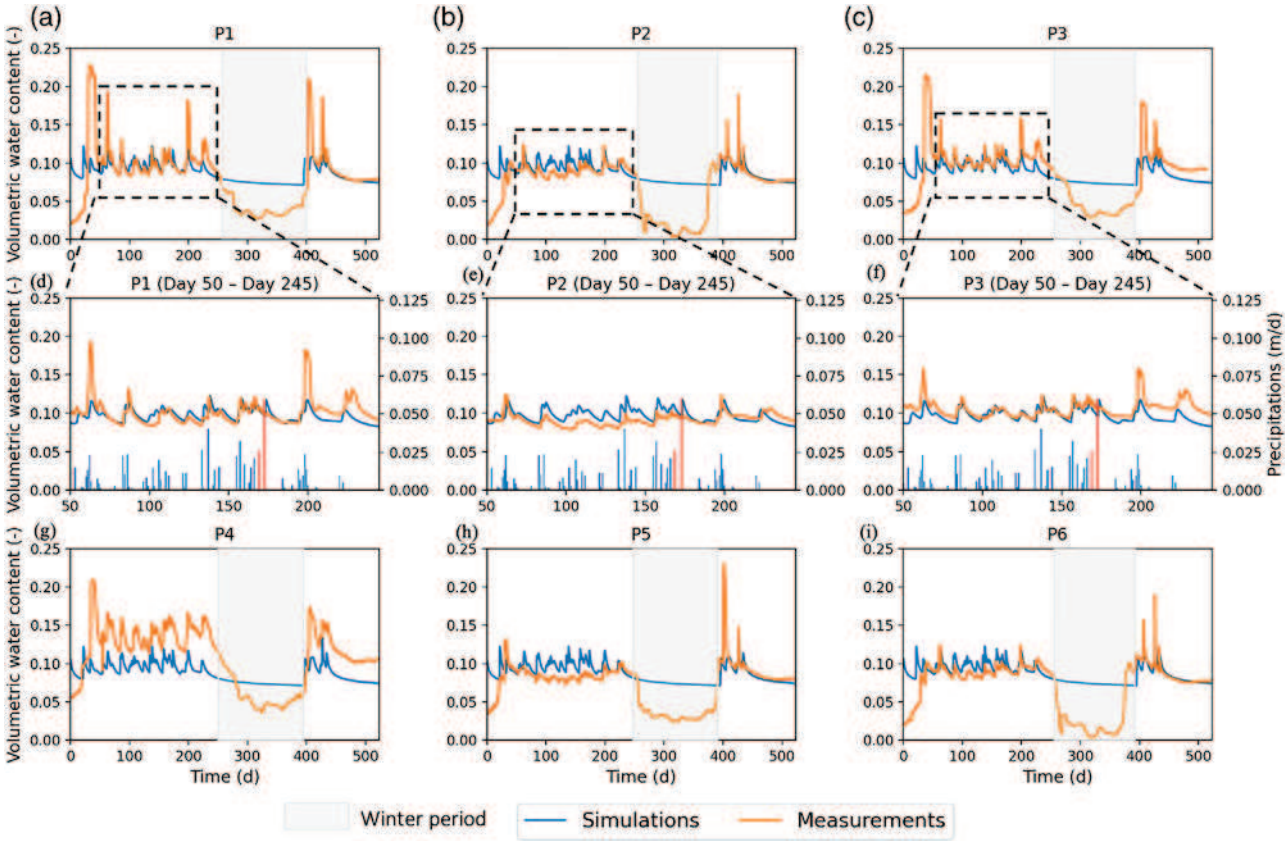

FIGURE 8 Simulated (blue) and measured (orange) volumetric water contents 0.80 m below the surface of the experimental waste rock pile between 4 Apr. 2016 (Day 0) and 13 Sept. 2017 (Day 523). Precipitations (blue) and large scale infiltration tests I-A and I-B (red) are represented for summer 2016 only (d, e, f)

simulated recovery percentage was smaller for test I-D and around 42% instead, but the measured recovery was 67%. The low recovery percentages measured in the field actually indicated an accumulation of water in the lysimeters before the water flew out of the systems and was collected (which was also confirmed by the high water contents measured in the lysimeters). Simulations did not account for lysimeters and simulated directly the outflow at the base of the waste rock pile.

4.4 | Validation for the 2016–2017 period

The calibrated hydrogeological properties were then used to simulate the hydrogeological response of the experimental waste rock pile for a period of approximately 17 mo (4 Apr. 2016 to 13 Sept. 2017), including two summers (Figure 8).

Between Day 0 and Day 42 (from 4 April to 16 May), and between Day 400 and Day 412 (from 9 to 21 May), the measured volumetric water contents increased significantly because of snowmelt and exceeded a degree of saturation S_r = 70% in some cases (porosity of the FCL = 0.30). Simulations differed significantly during this period because the snow cover was not simulated in the models. However, these large discrepancies lasted only for a few days and measured volumetric water contents decreased rapidly (within 5 d after the peak) to values around 0.11. During winter (Days 245–390), measured volumetric water contents decreased continuously because (a) there was no infiltration in the experimental waste rock pile (frozen surface), and (b) water contents probes only measured liquid water (Guo et al., 2018). Simulated water contents, however, remained around 0.07 because frost was not simulated in the models.

During summer 2016 (Days 50–241) and 2017 (Days 418–523), numerical simulations reproduced well the measured water contents variations, especially for P2 and P6, where the difference between the measured and simulated water contents never exceeded 0.02 (i.e., less than the precision of the GS3 sensors; Figure 8). Measured and simulated water contents variations were also very similar for P1 and P3, with differences generally less than 0.01 between Day 67 and Day 195 (Figures 8d, f). Larger precipitation events (such as the 3 d of precipitations observed on Day 195) sometimes induced a significant increase of the water contents (from 0.12 to 0.18) in the field, which was not always very well reproduced by the simulations (from Day 195 to Day 197). However, such

TABLE 4 Initial and bound values applied to the FCL sand during the optimization process. k_{sat} : Saturated hydraulic conductivity, α_{vG}, n_{vG}: van Genuchten (1980) fitting parameters

Bounds	Thickness	k_{sat}	α_{vG}	n_{vG}	Saturated water content
	m	m s^{-1}	m^{-1}		
Low bound	0.50	2.2×10^{-5}	0.10	1.05	0.20
Initial value	0.70	9.0×10^{-5}	2.44	3.89	0.30
High bound	1.12	1.0×10^{-3}	56.23	25.12	0.40

Note. k_{sat}, saturated hydraulic conductivity; α_{vG} and n_{vG}, van Genuchten (1980) fitting parameters.

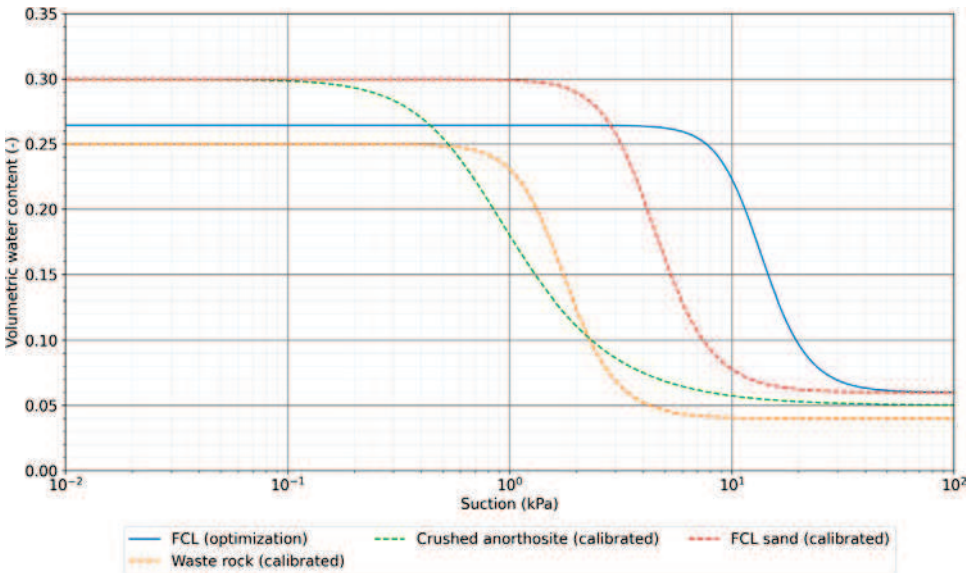

FIGURE 9 Calibrated and optimized water retention curves of the simulated materials. FCL, flow control layer

differences were limited to 5 d during summer 2016, and simulated water contents were otherwise very similar to measured results (<0.02 difference). The simulated wetting front arrival times at sensors P1 to P6 after each precipitation event were also very close to measured ones, with a maximum delay of 0.7 d. Differences between measured and calibrated water contents for sensor P4 were larger and around 0.04, which was consequent with the differences observed during calibration (see above). Also, water contents at sensor P5 were well reproduced during 2017 (see above) but were a bit less good during summer 2016, where measured water contents had a lower value around 0.07 and the peaks were limited with an amplitude of 0.01. On Day 442 (20 June 2017), an impermeable cover was installed at the surface of the experimental waste rock pile, therefore preventing any infiltration. During this period, measured and simulated water content tended to the same residual water content value of 0.07 after 60 d, indicating that the simulations reproduced well the drainage behavior of the FCL. For P3 and P4, the residual value of water content was slightly greater (0.09), which could correspond to a somewhat higher water retention capacity around those two locations.

Overall, the automated calibration of the numerical simulations based on only a few characteristic points (times t_1, t_2, and t_a at different locations) during large infiltration tests I-C and I-D appeared efficient to simulate the hydrogeological behavior of the experimental waste rock pile.

5 | FCL DESIGN OPTIMIZATION USING THE AUTOMATED BLACK-BOX APPROACH

The new automated calibration approach proposed here could also be used to optimize FCL design (such as material properties and cover thickness) to improve reclamation efficiency. This time, instead of using measured volumetric water contents to back calculate the in situ hydrogeological properties of the various materials, the algorithm was adapted to evaluate the properties of the FCL that would contribute to maximize the deviation of infiltration and minimize the infiltration of water in the reactive waste rock.

The algorithm was therefore adapted to compute water outflow in each lysimeter (instead of water contents variations

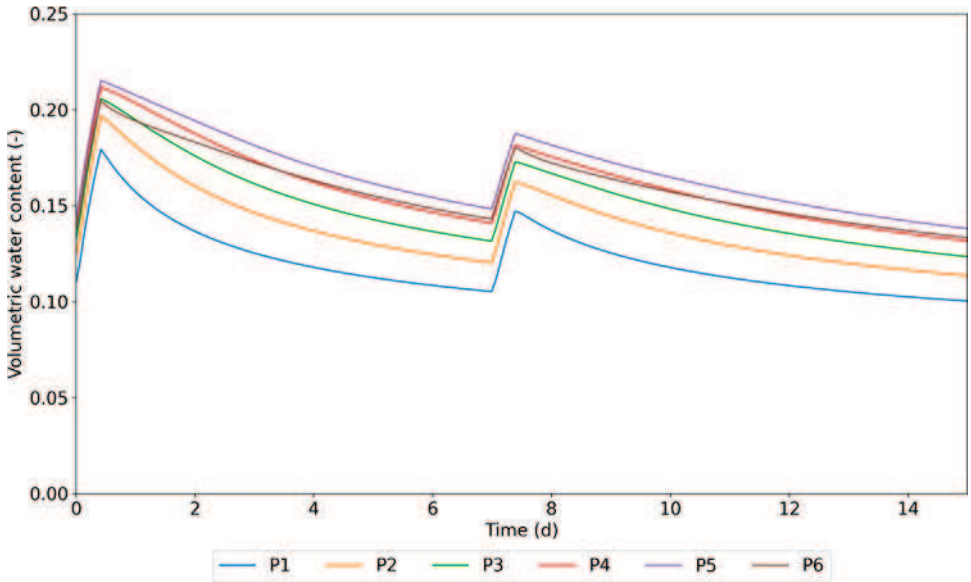

FIGURE 10 Water contents simulated 0.57 m below the surface obtained for the optimized hydrogeological properties. Time 0 corresponded to the start of test I-C

and arrival times in the calibration presented above), and the new objective was to minimize the sum of the outflows in lysimeters 1–5 (0–50 m). The cumulative volume was computed during the 7 d that followed the large infiltration test I-C. The new parameters adjusted by the black-box function were the thickness and the hydrogeological properties of the FCL (Table 4). The range of tested properties was chosen to respect practical and operational constraints. For example, considered FCL thicknesses were comprised between 0.4 and 1.4 m, and the FCL hydrogeological properties corresponded to realistic and easily available materials in this region. Input variables remained the same as in the previous simulations and included the saturated hydraulic conductivity, and the van Genuchten (1980) fitting parameters α_{vG} and n_{vG}. The porosity of the sand was also added along the input variable into the optimization process. Waste rock properties were kept constant during optimization and only the properties of the FCL were adjusted. The crushed anorthosite layer was removed to simplify the optimization process. Optimization was carried out for large infiltration tests I-C and I-D and then evaluated for a longer time (4 Apr. 2016 to 13 Sept. 2017).

Optimization showed that a material with a hydraulic conductivity of 1×10^{-3} m s^{-1} would be the most adapted material to build the FCL. The optimal porosity would be 0.265, and the air entry value and water entry value should be 8 and 22 kPa, respectively (Figure 9). This optimal material would be finer compared with the sand used on the experimental waste rock pile. Also, its air entry value would be greater than the waste rock water entry value (as recommended in previous research on a cover with capillary barrier effects; Broda et al., 2017; Fala et al., 2005; Ross, 1990). With this material, the optimum FCL thickness would be 0.77 m, which is slightly thicker than the one installed on the experimental waste rock pile.

The effectiveness of this optimum solution was 100%, corresponding to zero water flow in lysimeters 1–5. The cumulative outflow at the drainage face ($x = 60$ m) 7 d after test I-C was 18 m^3, which corresponded to 67% of the water applied at the surface of the experimental waste rock pile during test I-C (in other words, 67% of the infiltrated water was deviated laterally along the FCL). The maximum suction on the waste rock-FLC interface was 11 kPa, which was greater than the water entry value of the waste rock (6 kPa). The wetting front arrival time in the FCL 0.57 m below the surface during test I-C was around 9.84 h, which was faster than the measured and calibrated results (Table 3). The peak value increased with the distance along the slope, with a maximal water content at P5 (0.22), which was greater than P4 (0.21) to P1 (0.18) (Figure 10), therefore indicating some water accumulation along the FCL. The drainage was slower than measured and tended to a linear trend towards P6 corresponding to a slow vertical infiltration and important retention of water above the interface with the waste rock. The water contents simulated for sensors P1 to P6 were always above 0.15, thus maintaining the hydraulic conductivity of the FCL above 5×10^{-5} m s^{-1}, which explains the effective diversion and the large volumes of water leaving the boundary of $x = 60$ m.

Optimization results were evaluated on a longer period between 4 Apr. 2016 and 13 Sept. 2017 (Figure 11a). The general trends of the water content variations were similar to tests I-C and I-D, also indicating increasing water contents along the FCL. For example, the simulated water content at P5 was up to 0.04 greater than at P1. During the simulated 17 mo, 609 m^3 of water were applied on the top boundary resulting in

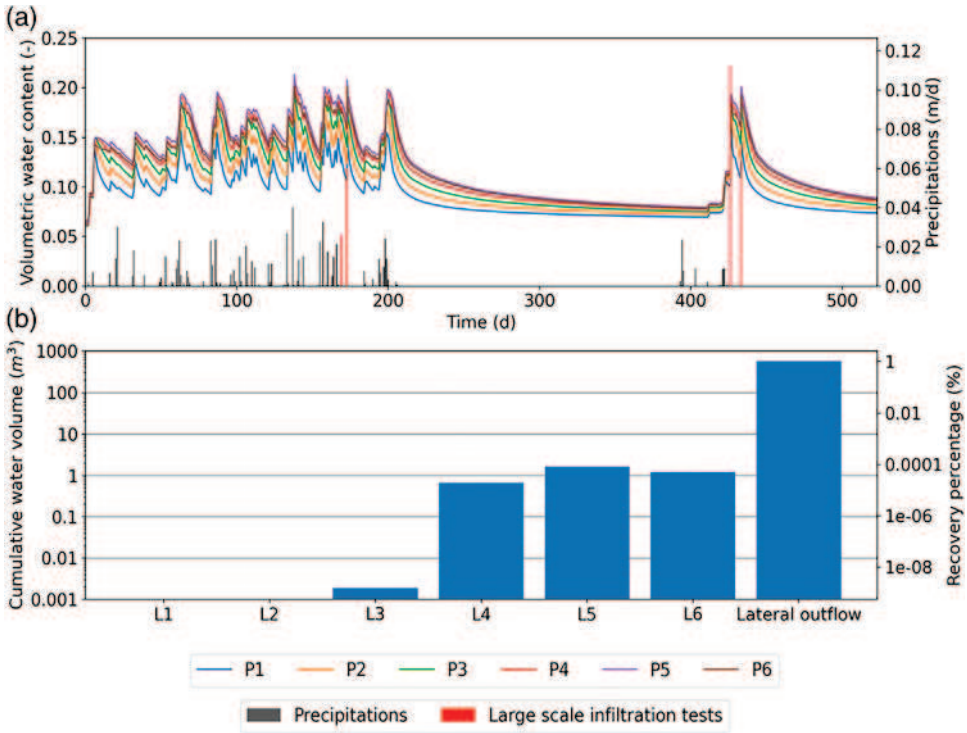

FIGURE 11 (a) Simulated water contents at 0.57 m with the optimized hydrogeological design between 4 Apr. 2016 and 13 Sept. 2017. Precipitations (in gray) and large-scale infiltration tests (in red) are also shown. (b) Cumulative water volume at each lysimeter after 17 mo of simulations. $x = 60$ m corresponds to the lateral outflow exiting the experimental waste rock pile. Note that both cumulative water volumes and recovery percentages are given in logarithmic scales

a total lateral deviation of 446 m^3 (73%). Less than 0.012 m^3 were observed in the lysimeters so the majority of the remaining 163 m^3 of water was stored for the major part inside the FCL where only 53 m^3 was stored inside the waste rock (Figure 11b). Overall, the optimized design seemed promising by proposing an effective FCL during the 17 mo of the numerical simulation. Additional simulations would, however, be required to validate this design for other types of climatic conditions and to take into account climate change effects.

6 | DISCUSSION

Calibrations of hydrogeological numerical simulations of waste rock piles were typically carried out manually in previous research (Demers et al., 2013; Ramasamy et al., 2018). This approach generally gave good results but was time consuming and subjected to interpretation bias. The automated approach developed in this study could improve and accelerate the calibration process. The calibration algorithm was based on a limited number of sensors (five water content probes in the FCL and four others in the waste rock), a few characteristic values (two values per probe in the FCL and one value per probe in the waste rock for each infiltration event) and only two large infiltration test results. Calibration was deemed satisfactory and calibrated simulations were able to reproduce relatively well water content variations.

The main differences between calibrated and measured water contents were limited to a few probes and some particular periods. These local discrepancies could be explained by heterogeneities and local variations of the hydrogeological properties (particle size distribution, porosity). Calibration could be improved by dividing each material into subgroups to reproduce local changes and variability (Ababou et al., 1989).

Calibration considered input parameters (hydraulic conductivity and van Genuchten [1980] fitting parameters α_{VG}, n_{VG}) as independent variables, whereas in practice they are correlated (Aubertin et al., 2003; Hollenbeck & Jensen, 1998). Calibration could therefore have been improved by resolving the black-box using particle size distribution properties as entry values or by using analytical solutions to link particle sizes and hydrogeological properties (Aubertin et al., 2003; Chapuis & Aubertin, 2003; Hillel, 1998). Such approach could also contribute to select best fitted solutions in case of nonunique solutions (i.e., limit the risk for solutions that would match the measurements but represent unrealistic properties).

Increasing the number of selected characteristic points on the resulted water content curves could also have contributed to improving the calibration. However, an increase in the

characteristics point may increase their variance resulting in underfitting. An underfitting variation could also appear after a poor quality of the spectral filter due to the small variations that could decrease the representativity of the characteristic points. Constraining more input variables could also be a solution to decrease the uncertainties during the calibration process and increase the representativity of the characteristics points (Nearing & Gupta, 2018).

Finally, the black-box algorithm has several other computational options and capacities that were not used in this research. For example, a bi-objective algorithm could be defined as an account for both water contents variations and water outflows at the same time. A similar approach was for example used in hydrology to reproduced runoff and water infiltration along with the groundwater behavior, allowing significantly more precise numerical simulation calibration (Turunen et al., 2020). Also, a sensibility analysis of the input variables could contribute to define more accurate poll search and mesh size parameters, thus reducing computational times and improving (Audet & Kokkolaras, 2016).

7 | CONCLUSION

An experimental waste rock pile was built at the Lac Tio mine site to evaluate the performance of an inclined FCL to control water infiltration and limit contaminated mine drainage generation. Water content measurements during two large infiltration tests were used to calibrate numerical simulations using an automated black-box algorithm. Calibrated simulations were able to reproduce the hydrogeological behavior of the experimental waste rock pile during the tests and for 17 mo of field monitoring. The persistent differences were probably related to local heterogeneity or variation of the hydrogeological properties, whereas the procedure using the black-box approach remains promising and flexible. The automated calibration approach was, then, also adapted to optimize the FCL design. Results showed that water deviation could be improved by automatically modifying the thickness and the hydrogeological properties of the FCL, to propose an ideal result of 100% efficiency. More generally, the optimization process proposed in this article could facilitate mining reclamation design and hydrogeological numerical simulations calibration for a broad range of cover systems and climatic conditions.

CONFLICT OF INTEREST

The authors declare no conflict of interest.

ACKNOWLEDGMENTS

This research was supported by the Natural Sciences and Engineering Research Council of Canada (NSERC) and by the partners of the Research Institute on Mines and Environment (RIME). The authors would like to acknowledge Pr. Charles Audet and his coworker from the GERAD for the software Nomad and their recommendation.

AUTHOR CONTRIBUTIONS

Tom Crouzal: Conceptualization; Methodology; Writing-original draft; Writing-review & editing. Thomas Pabst: Supervision; Validation; Writing-review & editing

ORCID

Tom Crouzal https://orcid.org/0000-0002-2369-846X
Thomas Pabst https://orcid.org/0000-0003-1493-806X

REFERENCES

Ababou, R., McLaughlin, D., Gelhar, L. W., & Tompson, A. F. B. (1989). Numerical simulation of three-dimensional saturated flow in randomly heterogeneous porous media. *Transport in Porous Media*, *4*, 549–565. https://doi.org/10.1007/BF00223627

Abbaspour, K. C., Schulin, R., & van Genuchten, M. T. (2001). Estimating unsaturated soil hydraulic parameters using ant colony optimization. *Advances in Water Resources*, *24*, 827–841. https://doi.org/10.1016/S0309-1708(01)00018-5

Akcil, A., & Koldas, S. (2006). Acid mine drainage (AMD): Causes, treatment and case studies. *Journal of Cleaner Production*, *14*, 1139–1145. https://doi.org/10.1016/j.jclepro.2004.09.006

Alarie, S., Audet, C., Garnier, V., Le Digabel, S., & Leclaire, L. A. (2013). Snow water equivalent estimation using blackbox optimization. *Pacific Journal of Optimization*, *9*, 1–21.

Arsenault, R., & Brissette, F. (2016). Analysis of continuous streamflow regionalization methods within a virtual setting. *Hydrological Sciences Journal*, *61*, 2680–2693. https://doi.org/10.1080/02626667.2016.1154557

Aubertin, M., Bussière, B., & Bernier, L. (2002). *Environnement et gestion des rejets miniers: Manuel sur cédérom*. Presses Internationales Polytechnique.

Aubertin, M., Bussière, B., Bernier, L., Chapuis, R., Julien, M., Belem, T., Simon, R., Mbonimpa, M., Benzaazoua, M., & Li, L. (2002). La gestion des rejets miniers dans un contexte de développement durable et de protection de l'environnement. In *Proceedings of the Annual Conference of the Canadian Society for Civil Engineering* (pp. 317–326). Canadian Society for Civil Engineering.

Aubertin, M., Bussière, B., Pabst, T., James, M., & Mbonimpa, M. (2016). Review of the reclamation techniques for acid-generating mine wastes upon closure of disposal sites. In A. Farid, A. De, K. R. Reddy, N. Yesiller, & D. Zekkos (Eds.), *Geo-Chicago 2016* (pp. 343–358). American Society of Civil Engineers.

Aubertin, M., Cifuentes, E., Apithy, S. A., Bussière, B., Molson, J., & Chapuis, R. P. (2009). Analyses of water diversion along inclined covers with capillary barrier effects. *Canadian Geotechnical Journal*, *46*, 1146–1164. https://doi.org/10.1139/T09-050

Aubertin, M., James, M., & Maknoon, M. (2013). *Recommandations pour améliorer le comportement géotechnique et géochimique des haldes à stériles*. Paper presented at GeoMontreal 2013. Canadian Geotechnical Society.

Aubertin, M., Mbonimpa, M., Bussière, B., & Chapuis, R. P. (2003). A model to predict the water retention curve from basic geotechnical properties. *Canadian Geotechnical Journal*, *40*, 1104–1122. https://doi.org/10.1139/t03-054

Audet, C. (2014). A survey on direct search methods for blackbox optimization and their applications. In T. M. Rassias & P. Pardalos (Eds.), *Mathematics without boundaries: Surveys in pure mathematics* (pp. 31–56). Springer.

Audet, C., & Dennis, J. E. (2006). Mesh adaptive direct search algorithms for constrained optimization. *SIAM Journal on Optimization*, *17*, 188–217. https://doi.org/10.1137/040603371

Audet, C., & Hare, W. (2017). *Derivative-free and blackbox optimization*. Springer. https://doi.org/10.1007/978-3-319-68913-5

Audet, C., & Kokkolaras, M. (2016). Blackbox and derivative-free optimization: Theory, algorithms and applications. *Optimization and Engineering*, *17*, 1–2. https://doi.org/10.1007/s11081-016-9307-4

Awotunde, A. A., & Horne, R. (2011). A multiresolution analysis of the relationship between spatial distribution of reservoir parameters and time distribution of well-test data. *SPE Reservoir Evaluation & Engineering*, *14*, 345–356. https://doi.org/10.2118/115795-PA

Benzaazoua, M., Bussière, B., Demers, I., Plante, B., Pepin, G., Aubertin, M., Chouteau, M., Dawood, I., Intissar, R., Lessard, G., Monzon, M., Peregoedova, A., Zagury, G. J., Molson, J. W., & Laflamme, D. (2013). *Comportement géochimique et hydrogéologique des stériles de la mine Lac Tio* (Déchets, sciences et techniques 64). Institut de l'information scientifique et technique, Centre national de la recherche scientifique.

Bigdeli, K., Hare, W., & Tesfamariam, S. (2012). Configuration optimization of dampers for adjacent buildings under seismic excitations. *Engineering Optimization*, *44*, 1491–1509. https://doi.org/10.1080/0305215X.2012.654788

Bréard Lanoix, M.-L. (2017). *Caractérisation des propriétés hydrogéologiques de la couche de con-trôle des écoulements placée sur la halde à stériles expérimentale à la mine du Lac Tio* (Master's thesis, Polytechnique Montreal).

Bréard Lanoix, M. - L., Pabst, T., & Aubertin, M. (2020). Field determination of the hydraulic conductivity of a compacted sand layer controlling water flow on an experimental mine waste rock pile. *Hydrogeology Journal*, *28*, 1503–1515. https://doi.org/10.1007/s10040-020-02129-7

Broda, S., Aubertin, M., Blessent, D., Hirthe, E., & Graf, T. (2014). Improving control of contamination from waste rock piles. *Environmental Geotechnics*, *4*, 274–283. https://doi.org/10.1680/envgeo.14.00023

Broda, S., Aubertin, M., Blessent, D., Hirthe, E., & Graf, T. (2017). Improving control of contamination from waste rock piles. *Environmental Geotechnics*, *4*, 274–283. https://doi.org/10.1680/envgeo.14.00023

Brunner, P., & Simmons, C. T. (2012). HydroGeoSphere: A fully integrated, physically based hydrological model. *Groundwater*, *50*, 170–176. https://doi.org/10.1111/j.1745-6584.2011.00882.x

Carrera, J., Alcolea, A., Medina, A., Hidalgo, J., & Slooten, L. J. (2005). Inverse problem in hydrogeology. *Hydrogeology Journal*, *13*, 206–222. https://doi.org/10.1007/s10040-004-0404-7

Chapuis, R. P., & Aubertin, M. (2003). On the use of the Kozeny-Carman equation to predict the hydraulic conductivity of soils. *Canadian Geotechnical Journal*, *40*, 616–628. https://doi.org/10.1139/t03-013

Demers, I., Molson, J., Bussière, B., & Laflamme, D. (2013). Numerical modeling of contaminated neutral drainage from a waste-rock field test cell. *Applied Geochemistry*, *33*, 346–356. https://doi.org/10.1016/j.apgeochem.2013.02.025

Dimech, A., Chouteau, M., Aubertin, M., Bussière, B., Martin, V., & Plante, B. (2019). Three-dimensional time-lapse geoelectrical monitoring of water infiltration in an experimental mine waste rock pile. *Vadose Zone Journal*, *18*, 180098. https://doi.org/10.2136/vzj2018.05.0098

Doherty, J. (2015). *PEST—The book: Calibration and uncertainty analysis for complex environmental models*. Watermark Numerical Computing.

Doherty, J. (2018). *PEST, model-independent parameter estimation user manual* (7th ed.). Watermark Numerical Computing.

Dubuc, J. (2018). *Étude du comportement hydrogéologique d'une couche de contrôle des écoulements placée à la surface d'une halde à stériles expérimentale* (Master's thesis, Polytechnique Montreal).

Dubuc, J., Pabst, T., & Aubertin, M. (2017). *An assessment of the hydrogeological response of the flow control layer installed on the experimental waste rock pile at the Lac Tio mine*. Paper presented at GeoOttawa 2017. Canadian Geotechnical Society.

Emsellem, Y., & De Marsily, G. (1971). An automatic solution for the inverse problem. *Water Resources Research*, *7*, 1264–1283. https://doi.org/10.1029/WR007i005p01264

Fala, O., Molson, J., Aubertin, M., & Bussière, B. (2005). Numerical modelling of flow and capillary barrier effects in unsaturated waste rock piles. *Mine Water and the Environment*, *24*, 172–185. https://doi.org/10.1007/s10230-005-0093-z

Fienen, M. N., Muffels, C. T., & Hunt, R. J. (2009). On constraining pilot point calibration with regularization in PEST. *Groundwater*, *47*, 835–844. https://doi.org/10.1111/j.1745-6584.2009.00579.x

Fowler, K. R., Reese, J. P., Kees, C. E., Dennis Jr, J. E., Kelley, C. T., Miller, C. T., Audet, C., Booker, A. J., Couture, G., Darwin, R. W., Farthing, M. W., Finkel, D. E., Gablonsky, J. M., Gray, G., & Kolda, T. G. (2008). Comparison of derivative-free optimization methods for groundwater supply and hydraulic capture community problems. *Advances in Water Resources*, *31*, 743–757. https://doi.org/10.1016/j.advwatres.2008.01.010

Guay, C., Minville, M., & Braun, M. (2015). A global portrait of hydrological changes at the 2050 horizon for the province of Québec. *Canadian Water Resources Journal/Revue canadienne des ressources hydriques*, *40*, 285–302. https://doi.org/10.1080/07011784.2015.1043583

Guo, Y., Xu, S., & Shan, W. (2018). Development of a frozen soil dielectric constant model and determination of dielectric constant variation during the soil freezing process. *Cold Regions Science and Technology*, *151*, 28–33. https://doi.org/10.1016/j.coldregions.2018.03.006

Hawley, M., & Cunning, J. (2017). *Guidelines for mine waste dump and stockpile design*. CSIRO Publishing.

He, X., Sonnenborg, T. O., Jørgensen, F., Høyer, A. - S., Møller, R. R., & Jensen, K. H. (2013). Analyzing the effects of geological and parameter uncertainty on prediction of groundwater head and travel time. *Hydrology & Earth System Sciences Discussions*, *10*(3). https://doi.org/10.5194/hess-17-3245-2013

Hillel, D. (1998). *Environmental soil physics: Fundamentals, applications, and environmental considerations*. Elsevier.

Hollenbeck, K. J., & Jensen, K. H. (1998). Maximum-likelihood estimation of unsaturated hydraulic parameters. *Journal of Hydrology*, *210*, 192–205. https://doi.org/10.1016/S0022-1694(98)00185-1

Isebor, O. J., Durlofsky, L. J., & Ciaurri, D. E. (2014). A derivative-free methodology with local and global search for the constrained joint optimization of well locations and controls. *Computational Geosciences*, *18*, 463–482. https://doi.org/10.1007/s10596-013-9383-x

Le Digabel, S. (2011). Algorithm 909: NOMAD: Nonlinear optimization with the MADS algorithm. *ACM Transactions on Mathematical Software (TOMS)*, *37*, 1–15. https://doi.org/10.1145/1916461.1916468

Martin, V., Bussière, B., Plante, B., Pabst, T., Aubertin, M., Medina, F., Lanoix, M. - L. B., Dimech, A., Dubuc, J., & Poaty, B. (2017). *Hydrogeophysical monitoring of water infiltration and moisture content to assess the performance of mining reclamation covers view project detoxification of cyanide view project*. Paper presented at GeoOttawa 2017. Canadian Geotechnical Society.

Martin, V., Pabst, T., Bussière, B., Plante, B., & Aubertin, M. (2019). A new approach to control contaminated mine drainage generation from waste rock piles: Lessons learned after 4 years of field monitoring. In *Proceedings of the 18th Global Joint Seminar on Geo-Environmental Engineering*.

McCarter, M. K. (1990). *Design and operating considerations for mine waste embankments*. Society of Mining Engineers of AIME.

Minville, M., Cartier, D., Guay, C., Leclaire, L., Audet, C., Le Digabel, S., & Merleau, J. (2014). Improving process representation in conceptual hydrological model calibration using climate simulations. *Water Resources Research*, *50*, 5044–5073. https://doi.org/10.1002/2013WR013857

Molson, J. W., Fala, O., Aubertin, M., & Bussière, B. (2005). Numerical simulations of pyrite oxidation and acid mine drainage in unsaturated waste rock piles. *Journal of Contaminant Hydrology*, *78*, 343–371. https://doi.org/10.1016/J.JCONHYD.2005.06.005

Mugunthan, P., Shoemaker, C. A., & Regis, R. G. (2005). Comparison of function approximation, heuristic, and derivative-based methods for automatic calibration of computationally expensive groundwater bioremediation models. *Water Resources Research*, *41*, W11427, https://doi.org/10.1029/2005WR004134

Nearing, G. S., & Gupta, H. V. (2018). Ensembles vs. information theory: Supporting science under uncertainty. *Frontiers of Earth Science*, *12*, 653–660. https://doi.org/10.1007/s11707-018-0709-9

Neuman, S. P. (1973). Calibration of distributed parameter groundwater flow models viewed as a multiple-objective decision process under uncertainty. *Water Resources Research*, *9*, 1006–1021. https://doi.org/10.1029/WR009i004p01006

Pabst, T., Molson, J., Aubertin, M., & Bussière, B. (2017). Reactive transport modelling of the hydro-geochemical behaviour of partially oxidized acid-generating mine tailings with a monolayer cover. *Applied Geochemistry*, *78*, 219–233. https://doi.org/10.1016/j.apgeochem.2017.01.003

Peregoedova, A., Aubertin, M., & Bussière, B. (2013). *Laboratory measurement and prediction of the saturated hydraulic conductivity of mine waste rock*. Proceedings of the GeoMontreal.

Peregoedova, A., Aubertin, M., & Bussière, B. (2014). *Evaluation of the water retention curve of mine waste rock using laboratory tests and predictive models*. Geo Regina.

Plante, B., Benzaazoua, M., Bussière, B., Biesinger, M. C., & Pratt, A. R. (2010). Study of Ni sorption onto Tio mine waste rock surfaces. *Applied Geochemistry*, *25*, 1830–1844. https://doi.org/10.1016/j.apgeochem.2010.09.010

Poaty, B., Plante, B., Bussière, B., Benzaazoua, M., Pabst, T., Aubertin, M., Martin, V., Thériault, M., & Nadeau, P. (2018). Geochemical behavior of different waste rock configurations from the Lac Tio mine: Comparison between column tests and experimental waste rock pile results. In *Proceedings of Tailings and Mine Waste Conference* (pp. 811–821). Tailings and Mine Waste Conference.

Poeter, E., & Anderson, D. (2005). Multimodel ranking and inference in ground water modeling. *Groundwater*, *43*, 597–605. https://doi.org/10.1111/j.1745-6584.2005.0061.x

Ramasamy, M., Power, C., & Mkandawire, M. (2018). Numerical prediction of the long-term evolution of acid mine drainage at a waste rock pile site remediated with an HDPE-lined cover system. *Journal of Contaminant Hydrology*, *216*, 10–26. https://doi.org/10.1016/j.jconhyd.2018.07.007

Ross, B. (1990). The diversion capacity of capillary barriers. *Water Resources Research*, *26*, 2625–2629. https://doi.org/10.1029/WR026i010p02625

Tavakoli, R., Pencheva, G., Wheeler, M. F., & Ganis, B. (2013). A parallel ensemble-based framework for reservoir history matching and uncertainty characterization. *Computational Geosciences*, *17*, 83–97. https://doi.org/10.1007/s10596-012-9315-1

Trinchero, P., Beckie, R., Sanchez-Vila, X., & Nichol, C. (2011). Assessing preferential flow through an unsaturated waste rock pile using spectral analysis. *Water Resources Research*, *47*(7). https://doi.org/10.1029/2010WR010163

Trudinger, J., & Spitz, K. (2008). *Mining & sustainability: The three circles of sustainable development*. IIR Executive Development.

Turunen, M., Gurarslan, G., Šimůnek, J., & Koivusalo, H. (2020). What is the worth of drain discharge and surface runoff data in hydrological simulations? *Journal of Hydrology*, *587*, 125030. https://doi.org/10.1016/j.jhydrol.2020.125030

van Genuchten, M.Th. (1980). A closed-form equation for predicting the hydraulic conductivity of unsaturated soils. *Soil Science Society of America Journal*, *44*, 892–898. https://doi.org/10.2136/sssaj1980.03615995004400050002x

Zhou, H., Gómez-Hernández, J. J., & Li, L. (2014). Inverse methods in hydrogeology: Evolution and recent trends. *Advances in Water Resources*, *63*, 22–37. https://doi.org/10.1016/j.advwatres.2013.10.014

How to cite this article: Crouzal T Pabst T. A black-box automated approach to calibrate numerical simulations and optimize cover design: Application to a flow control layer constructed on an experimental waste rock pile. *Vadose Zone J*. (2021);*20:*e20130. https://doi.org/10.1002/vzj2.20130